

**Visualizing molecular unidirectional rotation**Kang Lin,<sup>1</sup> Qiyong Song,<sup>1</sup> Xiaochun Gong,<sup>1</sup> Qinying Ji,<sup>1</sup> Haifeng Pan,<sup>1</sup> Jingxin Ding,<sup>1</sup> Heping Zeng,<sup>1,2,\*</sup> and Jian Wu<sup>1,†</sup><sup>1</sup>*State Key Laboratory of Precision Spectroscopy, East China Normal University, Shanghai 200062, China*<sup>2</sup>*Synergetic Innovation Center of Quantum Information and Quantum Physics, University of Science and Technology of China, Hefei, Anhui 230026, China*

(Received 18 March 2015; published 13 July 2015)

We directly visualize the spatiotemporal evolution of a unidirectional rotating molecular rotational wave packet. Excited by two time-delayed polarization-skewed ultrashort laser pulses, the cigar- or disk-shaped rotational wave packet is impulsively kicked to unidirectionally rotate as a quantum rotor which afterwards disperses and exhibits field-free revivals. The rich dynamics can be coherently controlled by varying the timing or polarization of the excitation laser pulses. The numerical simulations very well reproduce the experimental observations and intuitively revivify the thoroughgoing evolution of the molecular rotational wave packet of unidirectional spin.

DOI: [10.1103/PhysRevA.92.013410](https://doi.org/10.1103/PhysRevA.92.013410)

PACS number(s): 32.80.Rm, 33.80.-b, 33.15.Bh, 42.65.Re

**I. INTRODUCTION**

Controlling the motion of a molecule by coherently manipulating the rotational wave packet using ultrashort laser pulses is significant for a large variety of processes, ranging from extreme ultraviolet radiation generation [1–3] and molecular orbital and structure imaging [4,5], to chemical reaction steering [6]. In addition to fixing the molecular axis in space [7], a molecule can be optically kicked to spin unidirectionally at terahertz frequency in the polarization plane of the excitation laser pulses [8–10]. Similar to the well-studied spin of an electron, the molecular unidirectional rotation (UDR) is the directional spin of the molecular rotational wave packet which is coherently controllable using ultrashort laser pulses. A molecule can be adiabatically accelerated to a very high rotation frequency of more than 10 THz by optical centrifuge [11–15] using an energetic picosecond pulse of rotating linearly polarized laser field, or impulsively kicked to rotate at a frequency of a few terahertz by the double-pulse [16–19] or chiral-multipulse [20,21] excitation schemes. The extremely fast UDR of a molecule is observed to break molecular bonds [11,12], rotationally Doppler or Raman shift the frequency of a circularly polarized light depending on the rotation sense [14,18], boost the ionization of a particular electronic state [16,20], and resist collisions [22]. The molecular UDR is also interesting because it deflects molecules [23], generates molecular vortices [24], and works as a molecular wave plate [25].

However, a comprehensive picture of the spatiotemporal evolution of the impulsively excited molecular UDR, which essentially serves as the basis of all the initiated applications, has been lacking for more than 10 years since its observation. On the one hand, the molecular UDR has been mostly observed in the frequency domain using a spectral narrow-band laser pulse [14] to well resolve the frequency dependence and consequently is of limited temporal resolution. On the other hand, the rotational Doppler shift of the carrier frequency of an ultrashort laser pulse [18] provides an adequate temporal resolution. Nevertheless, it is hard to trace the full evolution

of the molecular UDR since its observation demands a strong anisotropic molecular distribution. The strong-field Coulomb explosion imaging [26–29] using an ultrashort laser pulse overcomes these hurdles, providing a temporal resolution in the femtosecond range without requisition of anisotropic molecular distribution.

In this paper, we directly visualize the spatiotemporal evolution of an impulsively created unidirectionally spinning molecular rotational wave packet using the ion-ion coincidence Coulomb explosion imaging technique. Our experiments and the numerical simulations intuitively present us with rich spatiotemporal dynamics of a rotational wave packet of unidirectional spin. Depending on the timings and polarizations of the ultrashort laser pulses, the well-confined cigar- or disk-shaped rotational wave packet can be impulsively kicked to rotate clockwise or counterclockwise which afterwards disperses and exhibits field-free revivals owing to the time-dependent beating of the coherently populated rotational states. Our results strengthen our understanding of this fascinating quantum dynamics and will stimulate new applications.

**II. DIRECT VISUALIZATION OF UDR**

We create the molecular UDR by sequentially kicking the molecule with two linearly polarized ultrashort laser pulses [16–19], i.e., the alignment pulse polarized along the  $z$  axis at  $t = 0$  and rotation pulse polarized at  $\pm 45^\circ$  in the  $y$ - $z$  plane with respect to the alignment pulse at  $t = t_r$ , as schematically illustrated in Fig. 1. The instantaneous snapshots of the molecular rotational wave packet at various times  $t = t_p$  are taken by Coulomb exploding the molecule using a time-delayed circularly polarized (probe) pulse in a reaction microscope using COLTRIMS [30,31] (“Cold target recoil ion momentum spectroscopy”). The three pulses are obtained via beam splitting and polarization shaping of a linearly polarized femtosecond laser pulse (25 fs, 790 nm, 10 kHz, Femtolasers) generated from a multipass amplifier Ti:sapphire laser system; the pulses are focused onto the supersonic gas jet of  $N_2$  by a concave silver mirror. The peak intensities of the alignment, rotation, and probe pulses in the interaction region are measured to be  $5 \times 10^{13}$ ,  $5 \times 10^{13}$ , and  $1.3 \times 10^{15}$  W/cm<sup>2</sup>, respectively. The temporal duration of the

\*hpzeng@phy.ecnu.edu.cn

†jwu@phy.ecnu.edu.cn

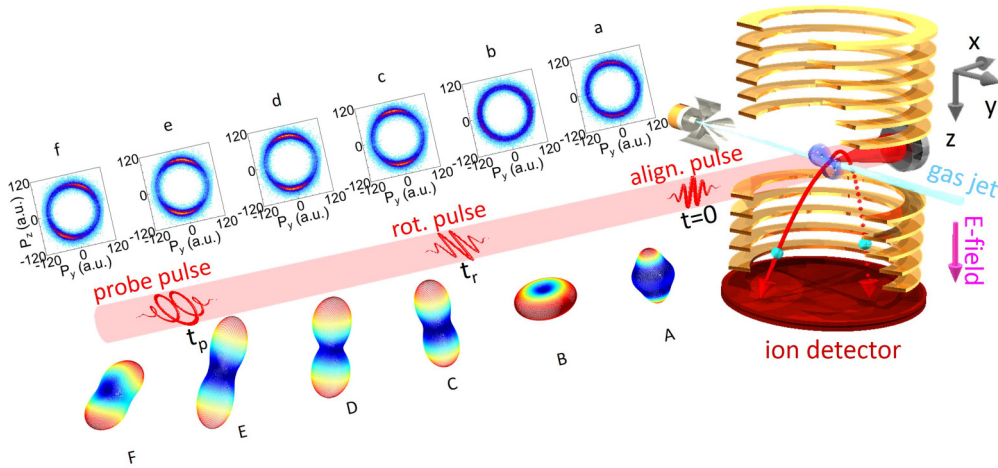


FIG. 1. (Color online) Experimental setup. The measurement is performed in an ultrahigh vacuum apparatus of COLTRIMS. A nitrogen molecule contained in a supersonic gas jet is impulsively aligned by an alignment pulse, which is subsequently kicked to rotate unidirectionally by a properly matched rotation pulse. An intense circularly polarized probe pulse with adjustable time delay is used to create a Coulomb explosion image of the evolution of the rotational wave packet. The insets a–f above the laser beam are the snapshots of the measured momentum distribution of the fragments of the Coulomb exploded nitrogen molecule, while the insets A–F below the laser beam are the simulated distributions of the rotational wave packet at various time delays.

alignment and rotation pulses are stretched to  $\sim 50$  fs, while the probe pulse is  $\sim 25$  fs. The photon-ionization-created fragment ions are guided by a weak homogeneous static electric field ( $\sim 10$  V/cm) to be detected by a time- and position-sensitive microchannel plate detector at the end of the spectrometer. We identify the fragment ions ejected from the same molecule based on the ion-ion coincidence. The extremely fast Coulomb explosion allows us to directly reconstruct the molecular axis from the relative momentum of the correlated fragment ions and hence the angular distribution of the rotational wave packet.

Since the  $N_2$  molecule is mostly ionized and fragmented when the molecular axis is parallel to the laser field vector, we restrict our data analysis for molecules in the polarization plane of the circularly polarized probe pulse in which the molecule is impulsively kicked to rotate unidirectionally. We characterize the evolution of the rotational wave packet by tracing the azimuth angle  $\phi$  between the molecular axis and the  $z$  axis in the  $y$ - $z$  plane. It is calculated using the projection of the measured momentum vectors of the fragment ions in the  $y$ - $z$  plane, i.e.,  $(P_y, P_z)$ . By step-by-step scanning the time delay of the probe pulse, a series of snapshots are taken to retrieve the full time-dependent evolution of the rotational wave packet. We note that the Coulomb explosion imaging is insensitive to the molecular anisotropy and the time resolution is comparable to the temporal duration of the probe pulse of tens of femtoseconds in our experiments.

Figure 2(a) displays the measured time-dependent angular distribution of  $N_2$  retrieved from the double-ionization-induced Coulomb explosion channel of  $N_2 + n\hbar\omega \rightarrow N^+ + N^+ + 2e$ , denoted as  $(N^+, N^+)$ . The  $(N^+, N^+)$  channel is selected using the momentum conservation of two detected fragment ions. The arrivals of the alignment and rotation pulses are indicated by the bright lines at time of  $t = 0$  and 8.6 ps, respectively. To increase the visibility and eliminate the bias induced by the nonperfect circularity of the probe pulse, we firstly normalize the total probability of the angular

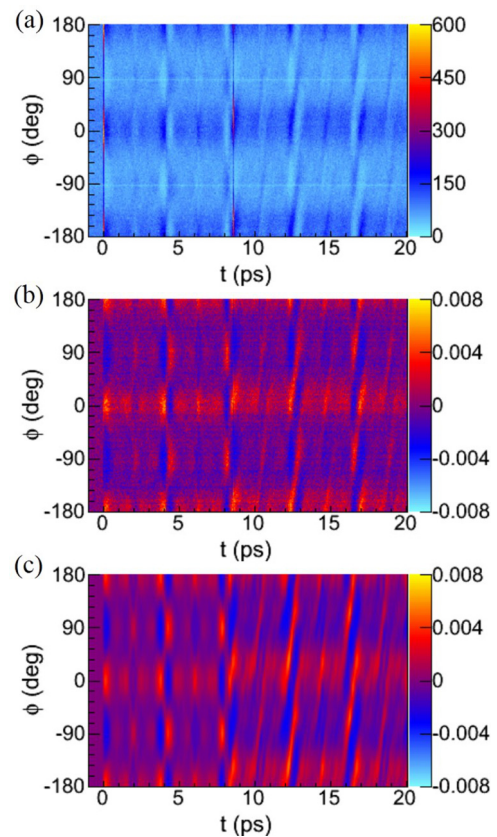


FIG. 2. (Color online) Time-dependent angular distribution. (a) Count plot of experimentally measured angular distribution of  $(N^+, N^+)$  fragments in the  $y$ - $z$  plane ejected from a doubly ionized nitrogen molecule as a function of the time delay of the probe pulse. (b) The normalized angular distribution of (a). (c) Numerically simulated angular distribution of the rotational wave packet in the  $y$ - $z$  plane spanned by the field vectors of the alignment and rotation pulses. The  $45^\circ$ -polarized rotation pulse arrives at the maximum of alignment revival at  $t = 8.6$  ps.

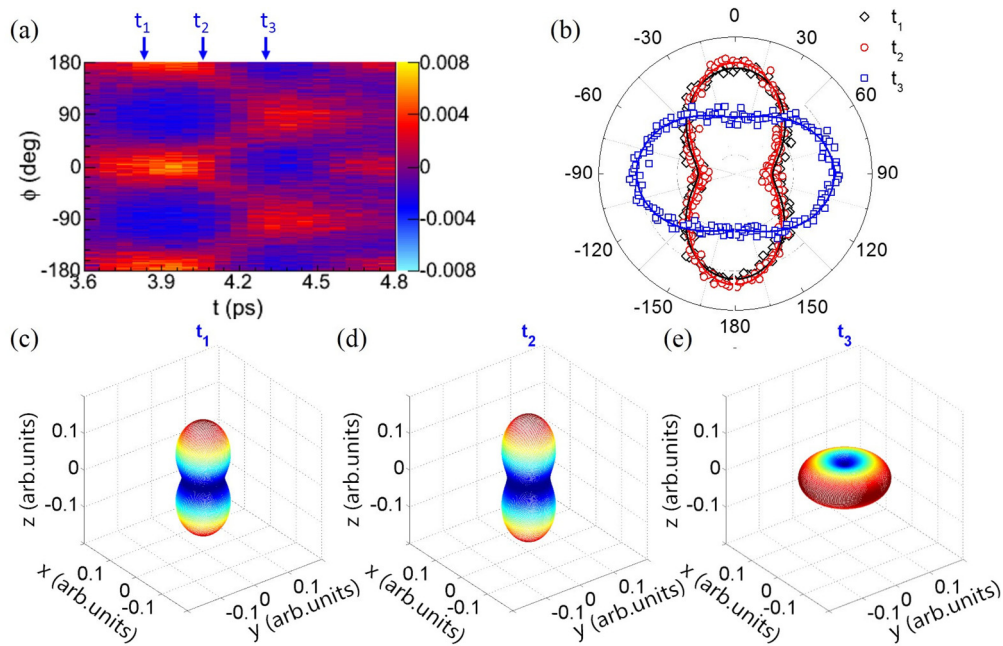


FIG. 3. (Color online) Angular distribution and rotational wave packet around  $t = 0.5t_{\text{rev}}$ . (a) Normalized angular distribution around  $t = 0.5t_{\text{rev}}$  taken from Fig. 2(b). (b) Polar plots of the angular distribution at  $t = t_1, t_2,$  and  $t_3$  as indicated in (a). (c–e) Numerically simulated rotational wave packet distributions at  $t = t_1, t_2,$  and  $t_3$ . The rotational wave packet evolves from cigar-shaped alignment to disk-shaped antialignment due to the sole excitation of the alignment pulse.

distribution to unity for each time delay and then subtract the averaged angular distribution before the arrival of the alignment pulse. Figure 2(b) illustrates the normalized angular distribution. Figure 2(c) shows the numerically simulated time-dependent angular distribution (see Appendix for details of the numerical simulations), which very well agrees with

the experimental measurement. The molecule firstly aligns to the polarization direction of the alignment pulse with an intense angular distribution well confined around  $\phi = 0^\circ$  and  $\pm 180^\circ$  at  $t = 0.2$  ps. The impulsively aligned rotational wave packet afterwards disperses and field-free evolves to alignment and antialignment at the (fractional) revivals owing to the

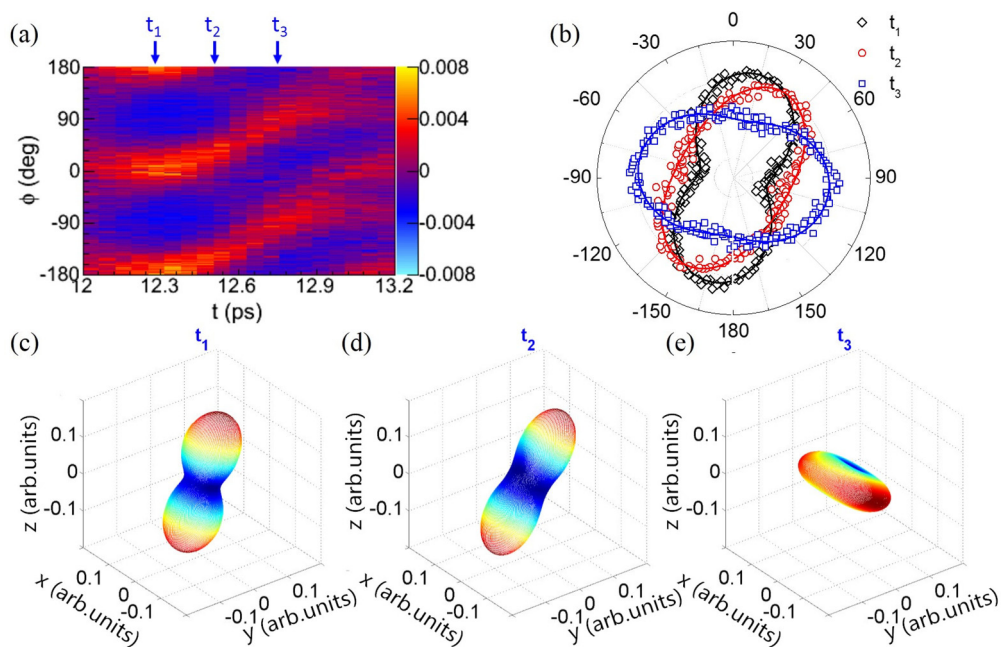


FIG. 4. (Color online) Angular distribution and rotational wave packet around  $t = 1.5t_{\text{rev}}$ . (a) Normalized angular distribution around  $t = 1.5t_{\text{rev}}$  taken from Fig. 2(b). (b) Polar plots of the angular distribution at  $t = t_1, t_2,$  and  $t_3$  as indicated in (a). (c–e) Numerically simulated rotational wave packet distributions at  $t = t_1, t_2,$  and  $t_3$ . The rotational wave packet transforms from cigar to disk shape and meanwhile rotates clockwise due to the sequential kicks of the alignment and rotation pulses.

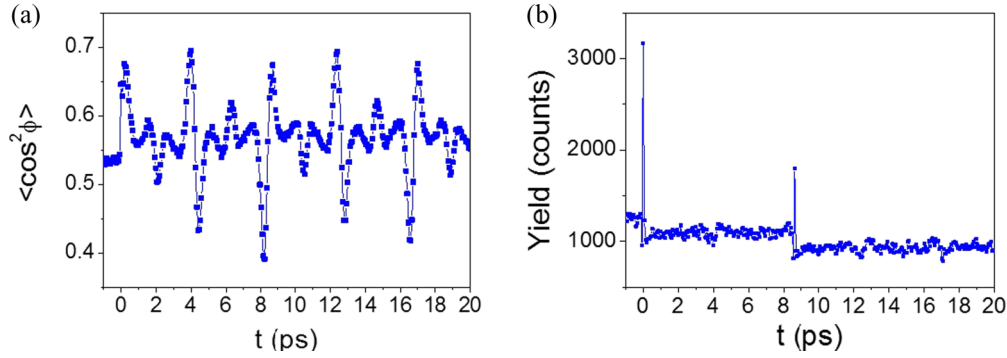


FIG. 5. (Color online) Time-dependent alignment degree and yield. (a) Measured  $\langle \cos^2 \phi \rangle$  in the  $y$ - $z$  plane, and (b) yield of the  $(N^+, N^+)$  fragments along the  $x$  axis as a function of the time delay of the probe pulse.

time-dependent phase beating of the coherently populated rotational states [32–34]. Figure 3(a) depicts the rapid quantum transformation from alignment to antialignment ( $\sim 500$  fs) around the half revival time of  $t = 0.5t_{\text{rev}}$ , where  $t_{\text{rev}} = 8.4$  ps is the full revival time of  $N_2$ . Figure 3(b) shows the polar plots of the angular distribution at  $t = t_1, t_2$ , and  $t_3$  indicated in Fig. 3(a). The corresponding three-dimensional rotational wave packets from our numerical simulations are presented in Figs. 3(c)–3(e), which agree well with the experiments and intuitively show the quantum evolution of the rotational wave

packet. The rotational wave packet at alignment maximum is cigar shaped [Figs. 3(c) and 3(d)] while it has a disk-shaped distribution [Fig. 3(e)] at antialignment maximum [35]. It evolves as a function of time but the angular distribution always up-down mirrors with respect to the polarization vector of the alignment pulse.

The rotation pulse is applied when the molecule is aligned along the  $z$  axis at  $t = 8.6$  ps. This impulsive torque unidirectionally rotates the cigar-shaped rotational wave packet to a frequency of terahertz [18,19]. Figure 4(a) depicts the detailed evolution of the angular distribution around  $t = 1.5t_{\text{rev}}$ . The corresponding polar plots at  $t = t_1, t_2$ , and  $t_3$  are shown in Fig. 4(b). As compared to that around  $t = 0.5t_{\text{rev}}$  [Fig. 3(a)], the angular distribution in Fig. 4(a) tilts as a function of time which directly illustrates the UDR of the molecule. The rotational wave packet rotates clockwise and meanwhile evolves from alignment to antialignment. As visualized in Figs. 4(c)–4(e), this joint motion leads to a rotating cigar or rotating disk of the rotational wave packet, agreeing well with the experimentally imaged angular distribution of the molecule in the  $y$ - $z$  plane as shown in Fig. 4(b). Due to the weak molecular anisotropy at the antialignment revival, this rotational wave packet of rotating disk was not observed in recent experiments [18,19] based on the rotational Doppler shift of the carrier frequency of a circularly polarized pulse. The animated spatiotemporal evolutions of the measured angular distribution (see Supplemental Material [36]) and the numerically simulated three-dimensional rotational wave packet (see Supplemental Material [36]) intuitively revivify the molecular UDR. It presents to us a full picture of the spatiotemporal evolution of an impulsively spun molecular rotational wave packet.

We notice that it is difficult to trace the molecular UDR by solely watching the temporal evolution of the  $\langle \cos^2 \phi \rangle$ , which is commonly used to qualify the degree of molecular alignment [37]. The average of  $\langle \cos^2 \phi \rangle = 0.5$  indicates the isotropic molecular orientation, while alignment and antialignment distributions result in values larger or smaller than 0.5, respectively [37]. As shown in Fig. 5(a), no noticeable difference is observed for  $\langle \cos^2 \phi \rangle$  before and after the kick of the rotation pulse at  $t = 8.6$  ps. The  $\langle \cos^2 \phi \rangle$  is little larger than 0.5 at  $t < 0$  owing to the bias of the nonperfect circularity of the probe pulse which is not eliminated here. It is predicted that the molecular spinning can confine the molecule in the

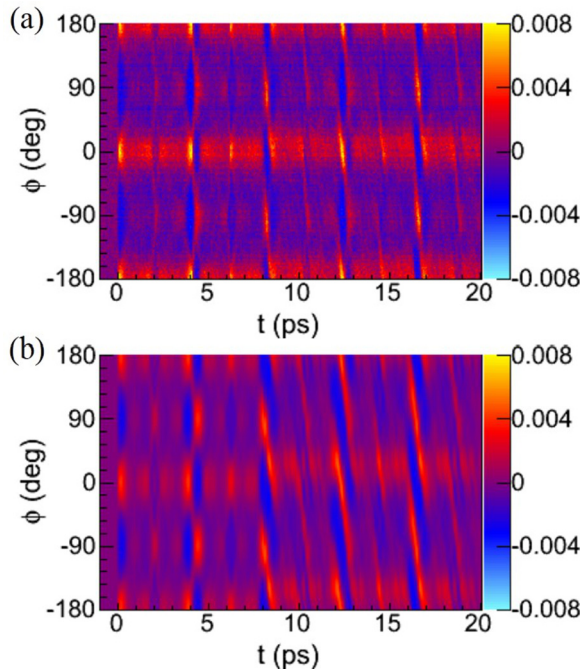


FIG. 6. (Color online) Time-dependent angular distribution. (a) Measured density plot of normalized angular distribution of  $(N^+, N^+)$  fragments in the  $y$ - $z$  plane as a function of the time delay of the probe pulse. (b) Numerically simulated angular distribution of the rotational wave packet in the  $y$ - $z$  plane spanned by the field vectors of the alignment and rotation pulses. The  $45^\circ$ -polarized rotation pulse arrives at the maximum of antialignment revival at  $t = 8.08$  ps. The other conditions are the same as Fig. 2. The time-dependent angular distribution oppositely tilts as compared to Fig. 2, indicating reversed rotation direction of the nitrogen molecule.

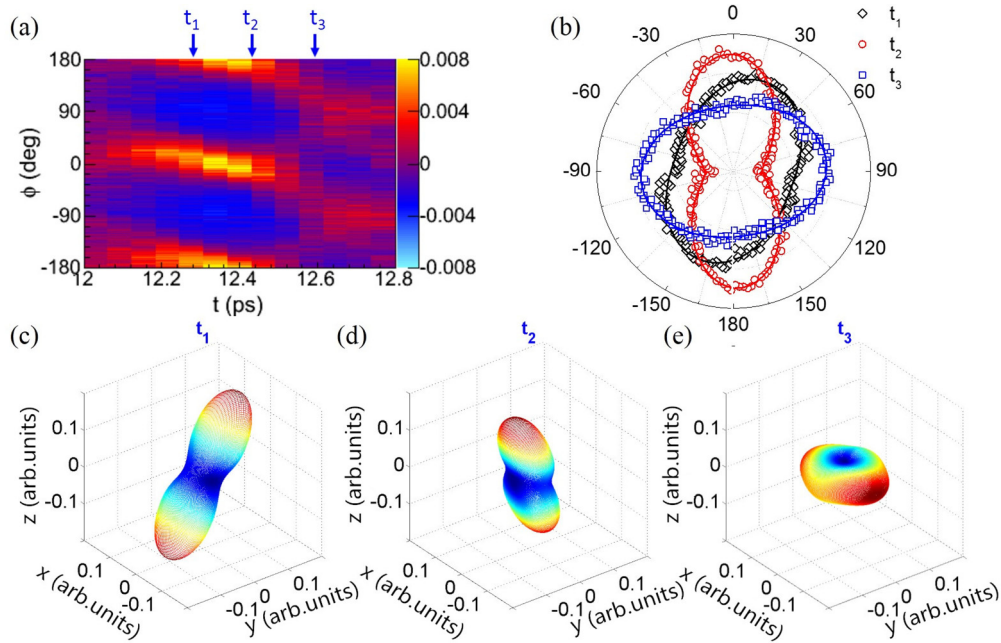


FIG. 7. (Color online) Angular distribution and rotational wave packet around  $t = 1.5t_{\text{rev}}$ . (a) Normalized angular distribution around  $t = 1.5t_{\text{rev}}$  taken from Fig. 6(a). (b) Polar plots of the angular distribution at  $t = t_1, t_2$ , and  $t_3$  as indicated in (a). (c–e) Numerically simulated rotational wave packet distributions at  $t = t_1, t_2$ , and  $t_3$ . The rotational wave packet transforms from cigar to disk shape and meanwhile rotates counterclockwise due to the sequential kicks of the alignment and rotation pulses.

plane spanned by the laser field vectors of the alignment and rotation pulses [9], which is indicated by the constant drop of the  $(N^+, N^+)$  yield along the  $x$  axis at  $t > 8.6$  ps, i.e., after the kick of the rotation pulse, as illustrated in Fig. 5(b).

### III. DISCUSSION

To demonstrate the robustness of our technique and test the validity of the data analysis, we adjusted the time delay of the  $45^\circ$ -polarized rotation pulse to  $t = 8.08$  ps when the molecule is antialigned with a disk-shaped rotational wave packet. Figures 6 and 7 depict the corresponding results. The numerical simulations agree well with the experimental measurements. As compared to Fig. 2, the time-dependent angular distribution of  $(N^+, N^+)$  tilts to the opposite direction, indicating reversed rotation direction of the molecule. It agrees with the recent rotational Doppler frequency shift measurements [18,19], and many more details of the rotational wave packet evolution are observed here. The rotation pulse kicks the molecule antialigned in the plane orthogonal to the vector of the alignment pulse and rotates counterclockwise the disk-shaped rotational wave packet, which afterwards can evolve into a rotating cigar shape owing to the phase beating of the coherently populated rotational states.

Alternatively, a counterclockwise rotating wave packet can be created by kicking the aligned molecule at  $t = 8.6$  ps using a rotation pulse polarized along  $-45^\circ$  with respect to the  $z$  axis in the  $y$ - $z$  plane. The corresponding results are displayed in Figs. 8 and 9. Interestingly, both experimentally and numerically, an entire upshift [Figs. 2(b) and 2(c), and Figs. 6(a) and 6(b)] or downshift [Figs. 8(a) and 8(b)] of the angular distribution is observed over the entire time after the

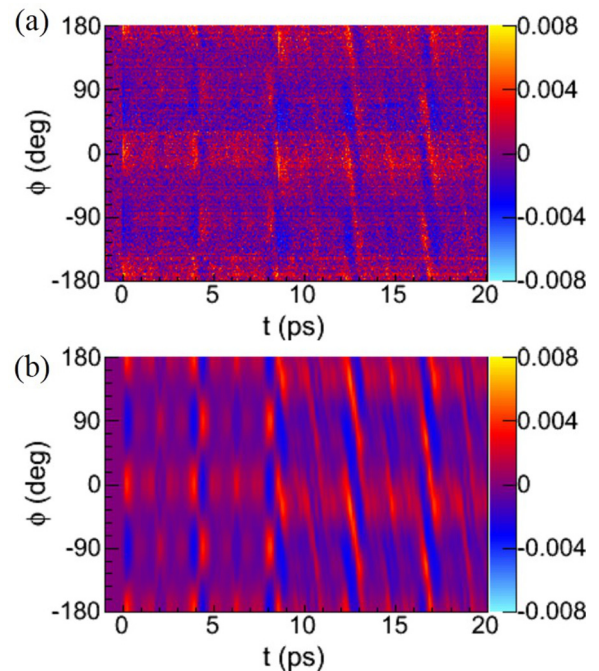


FIG. 8. (Color online) Time-dependent angular distribution. (a) Measured density plot of normalized angular distribution of  $(N^+, N^+)$  fragments in the  $y$ - $z$  plane as a function of the time delay of the probe pulse. (b) Numerically simulated angular distribution of the rotational wave packet in the  $y$ - $z$  plane spanned by the field vectors of the alignment and rotation pulses. The  $-45^\circ$ -polarized rotation pulse arrives at the maximum of alignment revival at  $t = 8.6$  ps. The time-dependent angular distribution oppositely tilts as compared to Fig. 2, indicating reversed rotation direction of the nitrogen molecule.

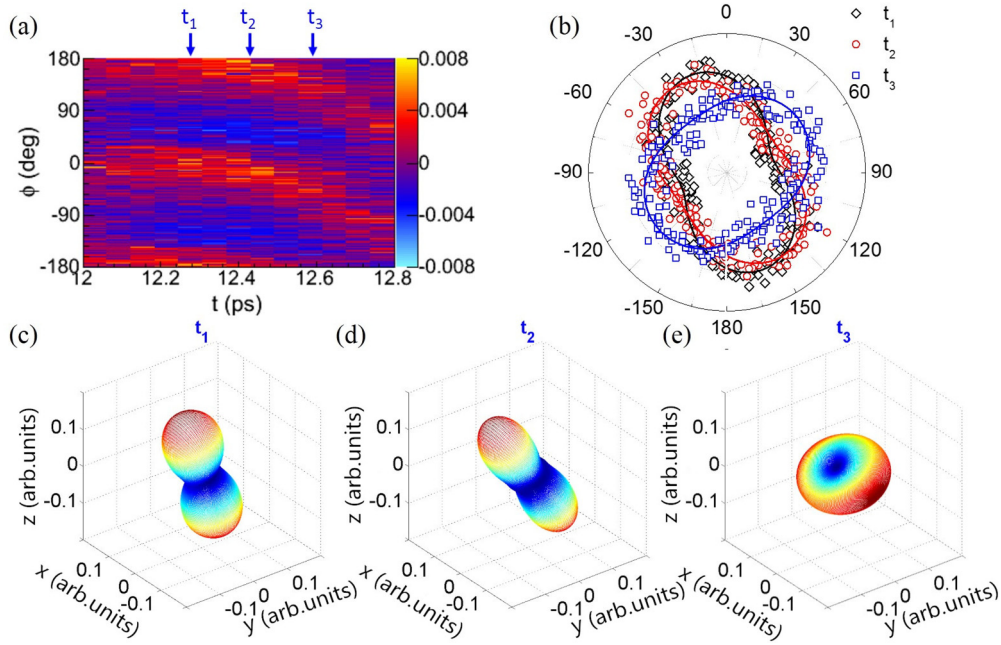


FIG. 9. (Color online) Angular distribution and rotational wave packet around  $t = 1.5t_{\text{rev}}$ . (a) Normalized angular distribution around  $t = 1.5t_{\text{rev}}$  taken from Fig. 8(a). (b) Polar plots of the angular distribution at  $t = t_1, t_2,$  and  $t_3$  as indicated in (a). (c–e) Numerically simulated rotational wave packet distributions at  $t = t_1, t_2,$  and  $t_3$ . The rotational wave packet transforms from cigar to disk shape and meanwhile rotates counterclockwise due to the sequential kicks of the alignment and rotation pulses.

kick of the rotation pulse. Regardless of the rotation sense of the molecule, the shift of the angular distribution solely depends on the polarization direction of the rotation pulse. It might be due to the incoherent alignment by the rotation pulse which swings the rotational wave packet to its polarization direction.

Differing from the classical-like nondispersing cogwheel state consisting of two or a few rotational states [15], here we directly visualize the rich quantum dynamics of a wide unidirectionally rotating molecular rotational wave packet impulsively kicked by ultrashort laser pulses. By varying the relative timing and polarization of the rotation pulse, we can coherently spin the rotational wave packet to different rotation senses. As compared to the very recently demonstrated UDR imaging using a specially designed two-dimensional ion-imaging configuration [38], the signal-to-noise ratio is significantly improved in our measurement by detecting the three-dimensional momenta of all the fragment ions ejected from a single molecule in coincidence.

#### IV. SUMMARY

In conclusion, a comprehensive spatiotemporal evolution of the double-pulse excited rotational wave packet of a UDR molecule is directly visualized using the ion-ion coincidence Coulomb explosion imaging technique. Our findings clearly reveal the field-free dispersion and the fractional revivals of an impulsively created rotational wave packet as a quantum rotor of unidirectional spin. By kicking the well-confined rotational wave packet at the alignment or antialignment maxima, a cigar- or disk-shaped rotational wave packet is spun to rotate clockwise or counterclockwise, which afterwards evolves into rotating cigar and disk shapes owing to the

quantum beating of the coherently populated rotational states of different energies. These full dynamics are very well intuitively reproduced by numerical simulations by solving the time-dependent Schrödinger equation of the rotational wave packet driven by ultrashort laser pulses. The thoroughgoing knowledge of the evolution of the field-free molecular UDR is anticipated to bring a great leap forward in research on molecular optical physics.

#### ACKNOWLEDGMENTS

We acknowledge helpful discussions with Ilya Sh. Averbukh, O. Faucher, and C. Hang. This work is supported by the National Natural Science Fund (Grants No. 11425416 and No. 11374103), the “Eastern Scholar” program, the NCET in University (Grant No. NCET-12-0177), a project from the Shanghai Science and Technology Commission (Grant No. 13QH1401400), and the “ShuGuang” project (Grant No. 12SG25).

#### APPENDIX: NUMERICAL SIMULATION

We model the UDR of a molecule by numerically solving the time-dependent Schrödinger equation [32,39]  $i\hbar\partial|\psi\rangle/\partial t = H_{\text{eff}}|\psi\rangle$  for the rotational state  $|\psi\rangle = \sum_{J,M} C_{JM}|J,M\rangle$ , where  $H_{\text{eff}} = B_0J(J+1) - 0.5\Delta\alpha\sin^2\theta(\varepsilon_z^2\cos^2\phi + \varepsilon_y^2\sin^2\phi + 2\varepsilon_z\varepsilon_y\sin\phi\cos\phi)$  is the effective Hamiltonian,  $B_0$  is the molecular rotational constant,  $\Delta\alpha$  is the polarizability difference between the components parallel and perpendicular to the molecular axis,  $\theta$  and  $\phi$  are the polar and azimuth angles of the molecular axis with respect to the  $x$  and  $z$  axes, and  $\varepsilon_y$  and  $\varepsilon_z$  are the envelopes of the laser field vector along the  $y$  and  $z$  axes, respectively. We first

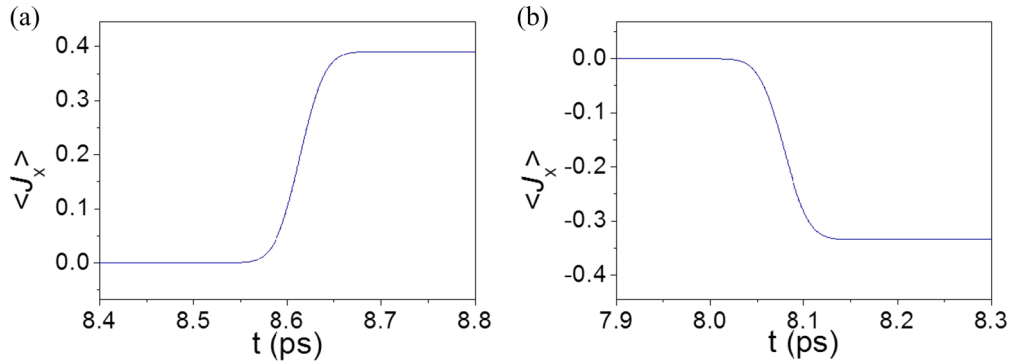


FIG. 10. (Color online) Time-dependent angular momentum. (a) Numerically simulated time-dependent angular momentum  $\langle J_x \rangle$  around the arriving time of the rotation pulse. The rotation pulse gradually spins up the molecule to rotate (a) clockwise ( $\langle J_x \rangle < 0$ ) and (b) counterclockwise ( $\langle J_x \rangle > 0$ ) in the  $y$ - $z$  plane when the rotation pulse arrives at the maxima of the (a) alignment and (b) antialignment revivals, respectively.

calculate the term  $P_{J_0 M_0}(\theta, \phi, t) = |\sum_{J, M} C_{JM}(t) Y_{JM}(\theta, \phi)|^2$  for each initial molecular rotational state  $|\psi(t=0)\rangle_{J_0 M_0} = |J_0, M_0\rangle$ , where  $Y_{JM}(\theta, \phi)$  are the spherical harmonic functions. We then assemble them by considering the temperature-dependent Boltzmann distribution of the initial rotational states, and eventually obtain the time-dependent probability density distribution of the rotational wave packet  $P(\theta, \phi, t)$ .

In the numerical simulation, the molecular parameters of  $N_2$  are  $B_0 = 1.98 \text{ cm}^{-1}$ ,  $\Delta\alpha = 1.0 \text{ \AA}^3$ . The initial rotational temperature of the  $N_2$  molecule is set to be 20 K, which is determined by matching the calculated arriving time of the first alignment maximum as well as the fractional revivals after the excitation of the alignment pulse to the experimental

observations. The parameters of the alignment and rotation pulses are chosen similar to the experiments. By coupling the rotational states of  $|J, M\rangle$  and  $|J \pm 2, M\rangle$ , the molecule is aligned by the alignment pulse, while the rotation pulse further couples different  $M$  states and spins the rotational wave packet. As shown in Fig. 10, the angular momentum of the rotational wave packet along the  $x$  axis  $\langle J_x \rangle$  gradually increases from zero to 0.39 or  $-0.33$  during the kick of the rotation pulse, which is constant after the end of the laser pulse owing to the angular momentum conservation. The larger amplitude of  $\langle J_x \rangle$ , when the rotation pulse matches the alignment maximum, compared to the antialignment maximum is consistent with the fact that the cigar-shaped rotational wave packet is more localized along the  $z$  axis as compared to the disk-shaped one in the  $y$ - $z$  plane.

- 
- [1] T. Kanai, S. Minemoto, and H. Sakai, *Nature* **435**, 470 (2005).  
 [2] J. Itatani, D. Zeidler, J. Levesque, M. Spanner, D. M. Villeneuve, and P. B. Corkum, *Phys. Rev. Lett.* **94**, 123902 (2005).  
 [3] N. Wagner, X. Zhou, R. Lock, W. Li, A. Wüest, M. Murnane, and H. Kapteyn, *Phys. Rev. A* **76**, 061403 (2007).  
 [4] J. Itatani, J. Levesque, D. Zeidler, H. Niikura, H. Pépin, J. C. Kieffer, P. B. Corkum, and D. M. Villeneuve, *Nature* **432**, 867 (2004).  
 [5] M. Meckel, D. Comtois, D. Zeidler, A. Staudte, D. Pavičić, H. C. Bandulet, H. Pépin, J. C. Kieffer, R. Dörner, D. M. Villeneuve, and P. B. Corkum, *Science* **320**, 1478 (2008).  
 [6] R. N. Zare, *Science* **279**, 1875 (1998).  
 [7] H. Stapelfeldt and T. Seideman, *Rev. Mod. Phys.* **75**, 543 (2003).  
 [8] J. Karczmarek, J. Wright, P. B. Corkum, and M. Ivanov, *Phys. Rev. Lett.* **82**, 3420 (1999).  
 [9] S. Fleischer, Y. Khodorkovsky, Y. Prior, and I. S. Averbukh, *New J. Phys.* **11**, 105039 (2009).  
 [10] S. Zhdanovich, A. A. Milner, C. Bloomquist, J. Floß, I. S. Averbukh, J. W. Hepburn, and V. Milner, *Phys. Rev. Lett.* **107**, 243004 (2011).  
 [11] D. M. Villeneuve, S. A. Aseyev, P. Dietrich, M. Spanner, M. Yu. Ivanov, and P. B. Corkum, *Phys. Rev. Lett.* **85**, 542 (2000).  
 [12] R. Hasbani, B. Ostoji, P. R. Bunker, and M. Yu. Ivanov, *J. Chem. Phys.* **116**, 10636 (2002).  
 [13] L. Yuan, S. W. Teitelbaum, A. Robinson, and A. S. Mullin, *Proc. Natl. Acad. Sci. USA* **108**, 6872 (2011).  
 [14] A. Korobenko, A. A. Milner, and V. Milner, *Phys. Rev. Lett.* **112**, 113004 (2014).  
 [15] A. Korobenko, J. W. Hepburn, and V. Milner, *Phys. Chem. Chem. Phys.* **17**, 951 (2015).  
 [16] K. Kitano, H. Hasegawa, and Y. Ohshima, *Phys. Rev. Lett.* **103**, 223002 (2009).  
 [17] Y. Khodorkovsky, K. Kitano, H. Hasegawa, Y. Ohshima, and I. S. Averbukh, *Phys. Rev. A* **83**, 023423 (2011).  
 [18] O. Korech, U. Steinitz, R. J. Gordon, I. S. Averbukh, and Y. Prior, *Nat. Photonics* **7**, 711 (2013).  
 [19] U. Steinitz, Y. Prior, and I. S. Averbukh, *Phys. Rev. Lett.* **112**, 013004 (2014).  
 [20] C. Bloomquist, S. Zhdanovich, A. A. Milner, and V. Milner, *Phys. Rev. A* **86**, 063413 (2012).  
 [21] J. Floß and I. S. Averbukh, *Phys. Rev. A* **86**, 063414 (2012).  
 [22] A. A. Milner, A. Korobenko, J. W. Hepburn, and V. Milner, *Phys. Rev. Lett.* **113**, 043005 (2014).  
 [23] E. Gershnel and I. S. Averbukh, *Phys. Rev. Lett.* **104**, 153001 (2010).  
 [24] U. Steinitz, Y. Prior, and I. S. Averbukh, *Phys. Rev. Lett.* **109**, 033001 (2012).  
 [25] A. G. York, *Opt. Express* **17**, 13671 (2009).

- [26] H. Sakai, C. P. Sufvan, J. J. Larsen, K. M. Hilligsoe, K. Hald, and H. Stapelfeldt, *J. Chem. Phys.* **110**, 10235 (1999).
- [27] P. W. Dooley, I. V. Litvinyuk, K. F. Lee, D. M. Rayner, M. Spanner, D. M. Villeneuve, and P. B. Corkum, *Phys. Rev. A* **68**, 023406 (2003).
- [28] I. A. Bocharova, A. S. Alnaser, U. Thumm, T. Niederhausen, D. Ray, C. L. Cocks, and I. V. Litvinyuk, *Phys. Rev. A* **83**, 013417 (2011).
- [29] X. Gong, M. Kunitski, L. Ph. H. Schmidt, T. Jahnke, A. Czasch, R. Dörner, and J. Wu, *Phys. Rev. A* **88**, 013422 (2013).
- [30] R. Dörner, V. Mergel, O. Jagutzki, L. Spielberger, J. Ullrich, R. Moshhammer, and H. Schmidt-Böcking, *Phys. Rep.* **330**, 95 (2000).
- [31] J. Ullrich, R. Moshhammer, A. Dorn, R. Dörner, L. Ph. H. Schmidt, and H. Schmidt-Böcking, *Rep. Prog. Phys.* **66**, 1463 (2003).
- [32] J. Ortigoso, M. Rodríguez, M. Gupta, and B. Friedrich, *J. Chem. Phys.* **110**, 3870 (1999).
- [33] R. A. Bartels, T. C. Weinacht, N. Wagner, M. Baertschy, C. H. Greene, M. M. Murnane, and H. C. Kapteyn, *Phys. Rev. Lett.* **88**, 013903 (2001).
- [34] V. Renard, M. Renard, S. Guérin, Y. T. Pashayan, B. Lavorel, O. Faucher, and H. R. Jauslin, *Phys. Rev. Lett.* **90**, 153601 (2003).
- [35] S. Fleischer, I. S. Averbukh, and Y. Prior, *J. Phys. B* **41**, 074018 (2008).
- [36] See Supplemental Material at <http://link.aps.org/supplemental/10.1103/PhysRevA.92.013410> for experimentally measured time-dependent evolution of the angular distribution of ( $N^+$ ,  $N^+$ ) fragments and numerically simulated three-dimensional rotational wave packet.
- [37] I. V. Litvinyuk, K. F. Lee, P. W. Dooley, D. M. Rayner, D. M. Villeneuve, and P. B. Corkum, *Phys. Rev. Lett.* **90**, 233003 (2003).
- [38] K. Mizuse, K. Kitano, H. Hasegawa, and Y. Ohshima, *Sci. Adv.* **1**, e1400185 (2015).
- [39] J. Wu and H. P. Zeng, *Phys. Rev. A* **81**, 053401 (2010).